Appl. Phys. A
DOI 10.1007/s00339-015-9066-7

Applied Physics A
Materials Science & Processing

RAPID COMMUNICATIONS

Thermal transport across graphene/SiC interface: effects of atomic bond and crystallinity of substrate

Man Li · Jingchao Zhang · Xuejiao Hu · Yanan Yue

Received: 26 November 2014 / Accepted: 20 February 2015

Abstract The effect of interatomic interaction between graphene and 4H-SiC on their interfacial thermal transport is investigated by empirical molecular dynamics simulation. Two magnitudes of interfacial thermal conductance (ITC) improvement are observed for graphene/4H-SiC interface interacting through covalent bonds than through van der Waals interaction, which can be explained by the bond strength and the number of covalent bonds. Besides, it is found that the ITC of covalent graphene/C-terminated SiC is larger than that Si-terminated SiC, which is due to the stronger bond strength of C–C than that of C–Si. The effect of crystallinity of the substrate is studied, and the result shows that the ITC of graphene/a-SiC is higher than that of graphene/c-SiC. These results are crucial to the understanding of thermal transport across graphene interfaces, which are useful for thermal design in graphene-based transistors.

1 Introduction

Graphene has attracted enormous attentions due to the unique physical properties and great potentials in semiconductor industrial applications [1, 2]. The super thermal conductivity of graphene or graphene ribbons, as high as several hundreds or thousands watts per meter per kelvin, has been verified by both experiments [3] and molecular dynamic (MD) simulations [4, 5]. It is promising that the future electronics will be released from the limitations of heat dissipation problems caused by hot spots, which may induce bad performance or even material failures in current silicon-based electronics. The ultrahigh thermal conductivity has also enabled the graphene nanocomposites as highly efficient thermal interface materials [6] by filling graphene in thermal grease matrix. However, the thermal performance of graphene-based thermal interface materials and nanoelectronic devices [7] is not solely determined by the intrinsic thermal conductivity of graphene. Thermal transport at the interfaces between graphene and substrates or matrix plays an important role because of the large contact area.

The substrate effect on in-plane phonon transport of graphene has been fully observed in supported single-layer graphene (SLG) and few-layer graphene (FLG). Using microfabricated devices, research group led by Dr. Li Shi found significantly suppressed thermal conductivity (k) of SLG exfoliated on silicon dioxide at room temperature [8] and similar results of FLG on an amorphous support from 100 K to 300 K [9]. These phenomena are attributed to the phonon leakages across the graphene/substrate interfaces and strong surface scattering of flexural phonon modes, which dominate the thermal conductivity of suspended graphene. The work of MD simulation provided consistent results with those experimental results obtained above [10] and a deeper insight into the underlying mechanism by conducting detailed analysis of phonon spectrum. The damping of the flexural acoustic (ZA) phonons was confirmed to be the main reason of the significant reduction in the thermal conductivity of supported graphene by an order of magnitude [11, 12]. Nevertheless, according to the

M. Li · X. Hu (✉) · Y. Yue (✉)
School of Power and Mechanical Engineering, Wuhan University, Wuhan, Hubei 430072, China
e-mail: xjhu@whu.edu.cn

Y. Yue
e-mail: yyue@whu.edu.cn

J. Zhang
Holland Computing Center, University of Nebraska Lincoln, Lincoln, NE 68588, USA

Published online: 04 March 2015

computation, 77 % of the heat is dissipated through the substrates directly in graphene field-effect transistor [7], which means the interfacial thermal transport is far more important than the intrinsic thermal conductivity of graphene, even with a significant suppression caused by interface interaction.

The quantity to evaluate the capability of the interfacial thermal transport is the interfacial thermal conductance (ITC) G, defined from the equation $Q = GA\Delta T$, in which Q is the net heat flux through the interface, A the area of the interface, and ΔT the temperature difference of the two sides of the interface. The ITC between graphene and its substrate has been investigated through both experiments and simulations, some of which are listed in Table 1. C. Dames et al. [13] initiated these experimental studies by utilizing the differential 3ω method, finding that the ITC between single-layer graphene and silicon dioxide (SiO_2) was 8×10^7 W/(m^2·K) at room temperature. Heinz et al. [14] adopted another method, i.e., optical pump pulse, and obtained the ITC of SLG/SiO_2 at 5×10^7 W/(m^2·K). Koh et al. [15] and Tang et al. [16] gave their results based on techniques of time-domain thermoreflectance and Raman spectroscopy, respectively. Tang et al. [16] also measured the ITC between graphene and silicon, far lower than the value of 1.33×10^7 W/(m^2·K) computed by Yang et al. [17] using MD simulation. The deviation between theoretical predictions and experimentally measured values stems from the quality of samples and the inherent errors of these techniques. On contrary with the situation of graphene/dielectrics interface, the results of ITC between graphene and metals are similar to the experiments [18] and simulations [19, 20]. However, considering the appearance of the technology for scalable production of epitaxial graphene on silicon carbide (SiC) [21] and the convenience of direct fabrication of graphene transistor from epitaxial graphene on SiC [22], the issue of thermal transport between graphene and SiC seems to have an urgent need to be investigated. Earlier, Calzolari et al. [23] performed a theoretical calculation based on first principles and the Landauer approach to study the ITC between graphene and SiC, whose results are 2.8×10^7 W/(m^2·K), a factor of 5 lower than the result of $\sim 1 \times 10^8$ W/(m^2·K) based on empirical MD simulations [24]. The common point shared by these studies is the van der Waals force responsible for adhering graphene to SiC substrate. But evidences revealed that the epitaxial graphene may be attached with its substrate [25] through covalent bond, which is much stronger than the van der Waals interaction. The ITC of covalently bonded interface is expected to be higher than that of the weakly bonded interface, but this quantitative enhancement remains mysterious. Another question about the effects of the crystalline and amorphous substrates also arises from the obvious distinction of the thermal properties of crystalline solids and amorphous solids.

Table 1 Examples of ITCs between graphene and substrates from literatures

Team	Methods	Materials	Typical results (300 K) W/(m^2·K)
Calzolari [23]	First principles and the Landauer approach	Graphene/BN	1.9×10^8
		Graphene/SiC	2.8×10^7
		Graphene/hydrogenated SiC	1.4×10^7
Dames [13]	Differential 3ω method	Graphene/SiO_2	8×10^7
Heinz [14]	Pump probe	Graphene/SiO_2	5×10^7
Koh [15]	Pump probe	Au/Ti/graphene/SiO_2	2.5×10^7
Luo [39]	MD simulation	Graphene/polymer	$\sim 6 \times 10^7$
Shi [44]	Raman spectroscopy	Graphene/BN	7.4×10^6
Tang [16]	Raman spectroscopy	Graphene/Si	183
		Graphene/SiO_2	266
Xu [24]	MD simulation	Graphene sandwiched between carbon buffer layer and 6H-SiC	1×10^8
Yang [17]	MD simulation	Graphene/Si	1.33×10^7
Yue [45]	Raman spectroscopy	Graphene/4H-SiC	1.9×10^4

In this work, we employ the MD simulation to study the interfacial thermal transport between graphene and SiC under different interatomic interactions and also explore the effect of substrate's crystallinity on ITC. The next section describes the methods including the principle and details about the MD simulation. In the result and discussion sections, the terminating side of substrate and the dependence of ITC between graphene and SiC on atomic bond will be presented, respectively. Finally, the effect of the crystallinity of substrate on the ITC of graphene/SiC interface is discussed.

2 Molecular dynamics simulation details

Molecular simulation (MD) is a powerful tool for studying nanoscale systems, benefiting from its direct and detailed description of atoms' information. In MD simulation, the individual atoms of silicon and carbon are treated as ideal mass points with no volume, interacting with each other through a given set of interatomic potentials. Since in our graphene/SiC system, the contribution of electron thermal transport to the overall interfacial thermal conductance (ITC) can be approximately evaluated from the interfacial

form of the Wiedemann–Franz law $GAR/T = L_0$ which had been validated by experiments, where G is the thermal conductance, AR the specific electrical resistance, T the temperature, and L_0 the Lorentz number 2.45×10^{-8} Ω W K^{-2} [26]. The contact resistance of graphene/SiC interface can be estimated as 0.063 Ω m^2 [27]. The electron interfacial thermal conductance can be computed as low as $\sim$ 1 W m^{-2} K^{-1}, far smaller than the overall ITC. Because the thermal energy dissipation mainly relies on the phonon coupling effect between C–C atoms and C–Si atoms, which means the contribution of the electrons to the thermal transport can be negligible, the electrons are not modeled in this work. The macroscopic variables can be deduced from coordination and velocities of atoms integrated numerically under the rule of classic mechanics. The prerequisite task of MD simulation is to build the correct geometry of atoms, including graphene and 4H-SiC in this case, as shown in Fig. 1(a). The effect of rotation of the covalent bonds between epitaxial graphene and SiC has been discovered [29]. According to the respective lattice constants of graphene and SiC, a commensurate structure is adopted here, in which 4H-SiC is reconstructed as $(6\sqrt{3} \times 6\sqrt{3})$ R30° and coincides with a 13 × 13 graphene supercell as shown in Fig. 1(b). This supercell is convenient for the adoption of periodical boundary condition. Besides, there are believable reports about the interfacial thermal transport simulations at graphene/6H-SiC, in which the same supercell was chosen [24, 28]. The system consists of 9316 atoms, with dimensions of 5.54 × 3.2 × 10 nm^3 ($x \times y \times z$). In the case of amorphous substrate, the dimensional lengths are set as the same with the crystalline substrate; however, the formation of the amorphous structure through high-temperature annealing is different, which has been mentioned in detail in our previous work [30].

The interatomic potential describes the interactions of atoms and is critically important in MD simulation. A widely used many-body potential proposed by Tersoff [31, 32] is adopted to describe the atomic interactions in SiC and graphene, as well as the covalent bonds between them.

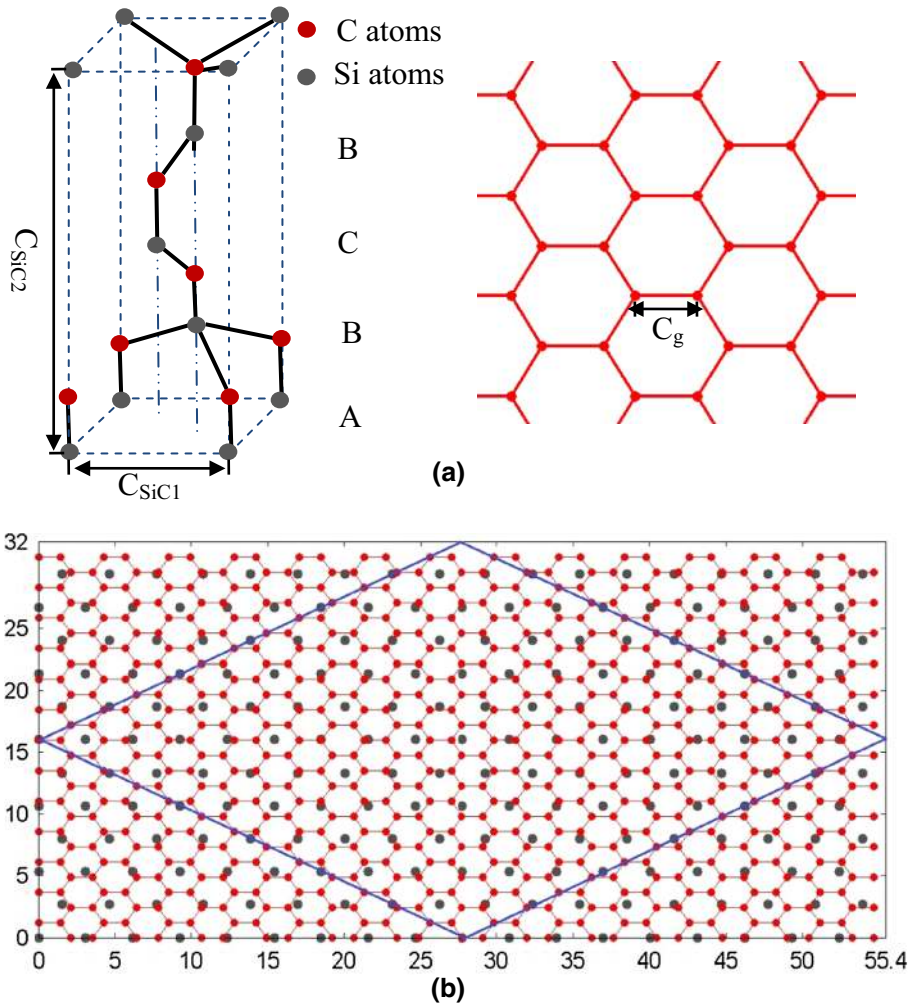

Fig. 1 **a** Geometric illustration of 4H-SiC and graphene. **b** The surface of the 4H-SiC oat the interface between graphene and 4H-SiC is reconstructed as $(6\sqrt{3} \times 6\sqrt{3})$ R30° and coincides with a 13 × 13 graphene supercell

When the interfacial bonds are the van der Waals interaction, the force field is described using a Lennard-Jones potential. The parameters of these potential functions are referenced from previous studies, which had simulated the corresponding materials successfully [31–33]. In spite of the deficiency of the original Tersoff potential parameters to simulate graphene, generating C–C bond with a length of 0.146 nm which was observed as 0.142 nm experimentally [34], it is adopted without optimization. Although the optimized Tersoff parameters [34] were proposed to describe the graphene and other carbon-related low-dimensional materials better, the improvement was built with sacrificing the accurate description about the silicon carbide. It is known that the Tersoff potential is a many-body potential. To simulate the covalent-bonded interface, two sides of this interface must be described by only one potential. Thus, if one side would be described best, the other side would be sacrificed. Therefore, the original Tersoff parameters are chosen for its overall accurate description of the internal interaction of SiC and the interfacial interaction between graphene and SiC. However, due to the overestimated bond length and the commensurate structure, the graphene on substrate would have slight corrugation.

All simulations in this work are performed by the large-scale atomic/molecular massively parallel simulator (LAMMPS) [35]. The system is initially stabilized at a constant temperature of 300 K and pressure of 1 bar for 0.8 ns at a time step of 0.2 fs (1 fs = 10^{-15} s). The time integration is performed on the Nose–Hoover style non-Hamiltonian equations of motion, which is designed to generate positions and velocities sampled from the canonical (NVT), isothermal–isobaric (NPT), and isenthalpic (NPT) ensembles [36]. And then, the artificial restrictions on atoms are released until the system is equilibrated. A heat flux via directly scaling the velocity of atoms while conserving momentum is added to the system by setting graphene as heat source and the bottom of SiC as heat sink; 400 ps is used for the system to reach steady state, and data averaging of another 400 ps is for ITC calculation. Since the method of heat introduction is not similar to that of the actual source of heat generation in a device, it would affect the interface thermal transport and vibrational properties of the atoms in an unknown way. However, it is challenging for the classical MD simulation to reproduce the scenario, and the computation cost would rapidly increase if considering this electron–phonon scattering process. An alternative is to use the sandwiched structure that put graphene in between two materials. This treatment also brings an issue about the phonon coupling effect directly between the substrate materials since the thickness of graphene is less than the cutoff distance of atomic potentials. When taking this into consideration, the sole phonon transport from graphene to substrate is hardly distinguished and how the coupling effects affect each other is complicated. Moreover, the study of graphene on substrate instead of sandwiched structure is more similar to the real scenario of graphene applications. Therefore, our selection of direct heating method in this work is a tradeoff treatment of considering both simulation techniques and the interest of this study.

3 Results and Discussions

3.1 Effect of the atomic bond: covalent and van der Waals

Different fabrication method of graphene interface determines the atomic interaction. For example, the direct epitaxial growth on a-SiC substrate features covalent bond [25], while exfoliation from graphite and oxidation graphite based on CVD method leads to the van der Waals force with substrate [37]. The covalent bond is much tighter and is good for heat dissipation. To date, it is still unknown about how the effect of atom interaction affects or say manipulates the interfacial thermal transport. In this simulation, the effect of interatomic interactions between graphene and SiC is studied on both C-terminated and Si-terminated surfaces.

Schematic of graphene on Si-terminated surface of SiC for the characterization of ITC is shown in Fig. 2. The equilibrium distance of graphene on Si- and C-terminated SiC at covalent interface in our work is 2.66 Angstroms and 2.33 Angstroms, respectively, similar to the reported work [25] as 2.58 Angstroms and 2.44 Angstroms. Their work studied the electronic properties of single- and double-layer graphene on Si- and C-terminated 6H-SiC where graphene is covalent bonded to the substrate just like our cases. The consistency of the structural analysis between our MD simulation and the ab initio simulation confirms the feasibility of our work. A steady-state method with constant heat flux is applied on graphene layer. Heat dissipates through the interface to the substrate. For the van der Waals system, the applied heat flux is 0.90 GW/m^2, which induces the temperature rise of less than 60 K in graphene, distinct and relatively small. For covalent bond, the heat flux is adjusted to 9.0 GW/m^2. According to the equation $Q = GA\Delta T$, the ITC can be calculated using the average temperature difference of the last 400 ps between the graphene and the nearest layer of SiC. The results are listed in Table 2. The error intervals are estimated based on a 95 % confidence interval from the temperature fluctuation of graphene. The magnitude of the computed values ranges from 10^7 W/(m^2·K) to 10^9 W/(m^2·K), depending on the specific interfacial interaction and the adjunct face of SiC to graphene.

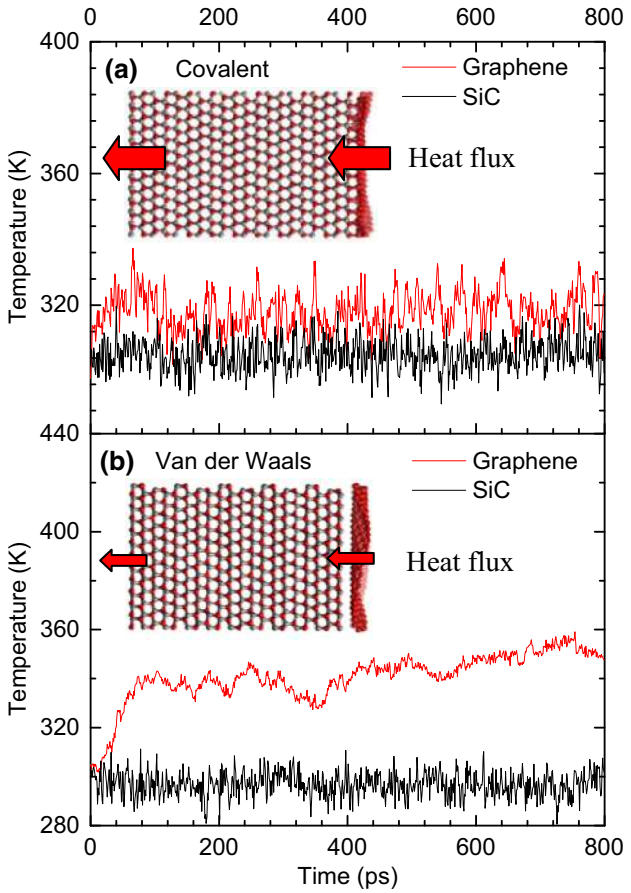

Fig. 2 **a** Illustration of the covalent-bonded model and the temperature evolution after a proper heat flux is added. **b** The illustration of the van der Waals model and the temperature evolution after a proper heat flux is added. In both models, the graphene is placed on the Si-terminated face

Table 2 Summary of the ITC between graphene and 4H-SiC, the error intervals are determined according the temperature fluctuation of graphene, based on a confidence interval of 95 %

ITC [10^7 W/(m^2·K)]	Covalent bonded	Van der Waals interaction
C-terminated	110 ± 7	2.33 ± 0.04
Si-terminated	64.8 ± 3	1.78 ± 0.02

Simulation results indicate that thermal transport from graphene to C-terminated 4H-SiC is better than to Si-terminated 4H-SiC for both atom interaction cases. For example, the ITC of covalent graphene/C-terminated SiC is $110 \pm 7 \times 10^7$ W/(m^2·K), around 1.7 times of ITC of covalent graphene/Si-terminated SiC which is $64.8 \pm 3 \times 10^7$ W/(m^2·K). The same case happens for van der Waals interactions. The ITC of graphene/C-terminated SiC is $2.33 \pm 0.04 \times 10^7$ W/(m^2·K), around 1.3 times of ITC of graphene/Si-terminated SiC, which is $1.78 \pm 0.02 \times 10^7$ W/(m^2·K). It shows that even for the same atom interaction, thermal transport across the same kind of atom bonded interface would be better. The relatively larger ITC of covalent graphene/C-terminated SiC interface can be explained by the better coupling effect of C–C atoms for phonon transmission than that of C–Si atoms. As the comparison of different atom interactions, it is found that the ITC of covalent graphene/C-terminated SiC is almost two magnitudes larger than that of the graphene/C-terminated SiC interface through van der Waals interaction. It can be observed that the equilibrium distance for covalent bond graphene on Si- and C-terminated SiC is 2.66 Angstroms and 2.33 Angstroms, respectively, while for van der Waals graphene interfaces 3.91 Angstroms and 3.84 Angstroms. The equilibrium distance of the van der Waals interface is much longer than the bond length of C–C bond and C–Si bond, both of which are less than 2 Angstroms. The longer distance impedes the formation of covalent bonds, makes the interaction weaker, and thus reduces the ITC. From the comparison of the distances and the ITC for different cases, the negative correlation of them can be justified. Besides, the covalent-bonded graphene/C-terminated SiC interface features high bond energy ($\sim$ 3.6 eV [38]), while the C–C energy constant of LJ potential is 0.00313 eV. The energy constants of the LJ potential have almost linear relationship with the ITC from the study of Luo et al. [39]. Theoretically, the ITC of covalent interface should be 1000 times larger than that of van der Waals interface despite the difference of the bond stiffness. It needs to be noticed that this improvement could be limited by possible failure of the linear relationship when the bond energy is large and relatively less covalent bonds than expected between adjacent materials. Unlike the long-distance interaction in van der Waals case, in which all the carbon atoms interact with the substrate under the Lennard-Jones potential with a cutoff distance of 10 Angstroms, the number of the carbon atoms bonded to SiC is much less because of the short cutoff distance of 2.2 and 2.5 Angstrom, respectively, for C–C bonds and C–Si bonds as well as the difference in surface atom density of graphene and SiC. As the number of covalent bonds during the simulation dominates ITC, the analysis of number of covalent bonds is conducted by using the radial distribution function (RDF), as shown in Fig. 3. The area under the first peak corresponds to the number of the coordinate number of the atom and is defined as $n = 4N\pi \int_{r_1}^{r_2} r^2 g(r) dr/V$, where $g(r)$ is the RDF, N the number of atoms, V the volume of system, r_1 the lower bound of the first peak, and r_2 the upper bound of the first peak. For van der Waals systems, the coordinate number of graphene atoms is 3, meaning that there are three atoms around each carbon atom in graphene. While for covalent systems, it is found that this number is 3.15976 and 3.13437 for C-terminated and Si-terminated

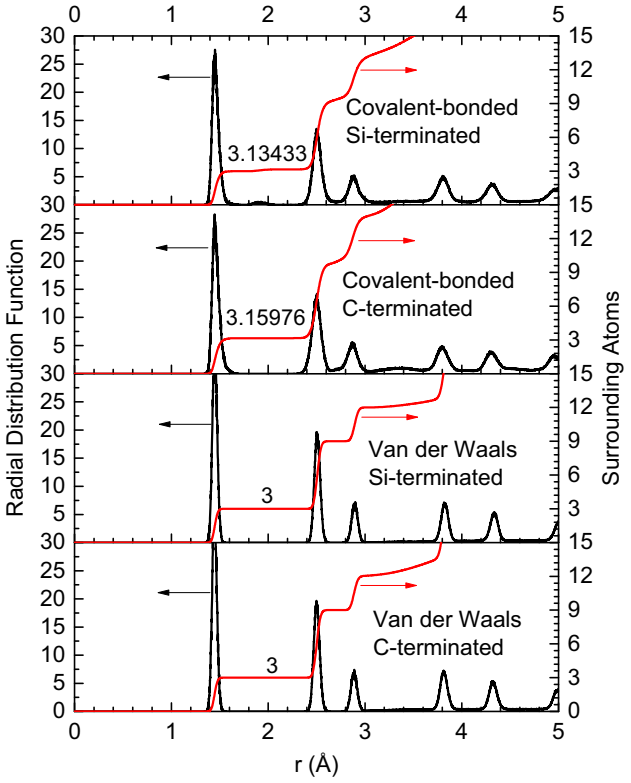

Fig. 3 Characterization of the local atomic environment of the graphene in our systems. The black line is the radial distribution function of the graphene, while the red line means the number of the surrounding atoms per atom in graphene

cases, respectively. From the decimal parts (0.15976 and 0.13437), one can derive the number of covalent bonds between graphene atoms and substrate atoms. That is, by multiplying the total number of graphene atoms of 676, the number of covalent bonds between graphene and substrate can be calculated as 108 and 91. Accordingly, 16 % and 13.4 % of carbon atoms in graphene forms covalent bonds for C–C and C–Si, respectively. As large amount of atoms in graphene is not in covalent bond with SiC, it is reasonable that the ITC values for the covalent bond interface are two order magnitude larger than van der Waals rather than three order magnitude larger according to the bond energy analysis. Compared with the experimental results listed in Table 1, it can be found that the ITC at the covalent interface is much higher. In experiment, it is much more difficult to fabricate the "pure" covalent graphene/substrate interfaces. It is caused by the experimental limitations such as the defects in graphene, some chemical residues at the graphene surface, and so on. Even more or less local thermal stress or hot spot appeared in the fabrication process would break the covalent bond at the interface. Therefore, it is hardly to get the order of $\sim 10^9$ W/m^{2}K for the interface thermal conductance in experimental characterization. In our simulation, it is an ideal structure without any defects or chemical residues, and it is not strange to get this theoretically high thermal transport property.

The larger ITC between graphene and C-terminated SiC than Si-terminated SiC can be partly explained by the smaller number of C–Si bonds than C–C bonds. Besides, the thermal coupling effect between C–C bond and C–Si bond can be analyzed through bond energy: The C–Si bond has the weaker strength of 3.3 eV [38] comparing with the C–C bond of 3.6 eV [38]. From the above analysis, the two main reasons responsible for different ITCs in Table 2 are the difference in the bond strength of different atoms under different interaction forces and the number of bonds formed in covalent systems.

Phonon spectral analysis is further conducted to understand simulation results. The phonon density of states (DOS) from the discrete Fourier transform of velocity autocorrelation function can be obtained by: $g(\omega) = \int e^{i\omega t}\langle\vec{v}(t)\vec{v}(0)\rangle/\langle\vec{v}(0)\vec{v}(0)\rangle dt$, where $\vec{v}(t)$ is velocity vector of an atom, and $\vec{v}(0)$ is the initial velocity vector. The angular brackets denote an average over the canonical ensemble. Since the covalent bonds between C atoms and Si atoms inside SiC is strong and has been well understood, the internal layer-to-layer thermal transport inside SiC is not considered in this work. Due to the intrinsic characteristics of the Tersoff and LJ potential, the interaction between graphene and the second nearest layer of the SiC is far weaker than the nearest layer. As a result, to analyze the phonon DOS of the sole nearest layer of the SiC will help us focus at the interface. Figure 4(a) shows the velocity autocorrelation functions (VAF) of the supported graphene on Si-terminated 4H-SiC through van der Waals interaction converging to zero when the time is more than 0.5 ps, which means the perturbative forces disrupt the perfect oscillation of atoms quickly and VAF during 1 ps is long enough in our cases for calculating the phonon DOS. The black line and blue line indicate the VAFs of graphene and Si atoms layer adjacent to graphene, respectively. Figure 4(b) shows the calculation results of DOS. Two peaks exist at the frequency of 12.0 THz and 29.3 THz for phonon DOS of the adjacent Si atoms layer (blue line), and the phonon DOS of graphene has a broader distribution. According to the diffusive mismatch model, all phonons striking the interface are scattered once (elastically) and are then emitted into the adjoining substances with a probability proportional to the phonon density of states in the respective substances. The overlap in the phonon DOS can be used to estimate the transmission of phonons across the interface through elastic scattering [40, 41]. The larger overlap area of the phonon DOS of the two sides was successfully used to explain the enhanced interfacial

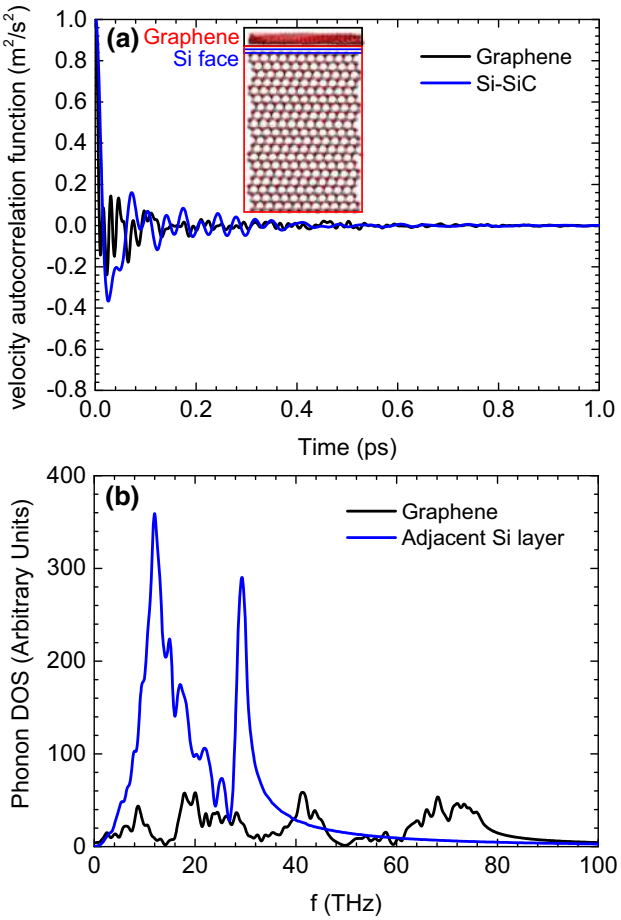

Fig. 4 **a** Velocity autocorrelation functions of graphene (*black*) and the adjacent Si atoms layer in SiC (*blue*). **b** The phonon DOS of the adjacent Si atoms layer (*blue*) and graphene (*black*)

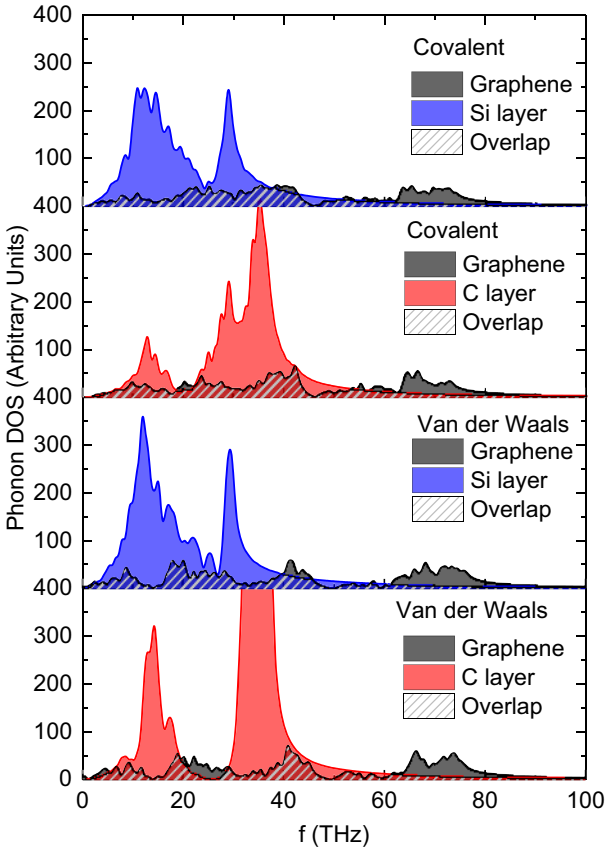

Fig. 5 Phonon DOS of graphene and its adjacent atoms layer of SiC with different terminated face under different interfacial interaction

thermal conductance in Ref. 41 and 42. Figure 5 demonstrates the phonon DOS of graphene and the adjacent atoms layer and their overlap area under van der Waals interaction and covalent bonding. The phonon DOS of adjacent C atoms layer shows a strongly two-peak feature and overlaps graphene's phonon DOS from 0 THz to 20 THz and from 30 THz to 60 THz, while the phonon DOS of adjacent Si atoms layer has a larger mismatch at the high frequency. Under the interaction of covalent bonding, The intensity of the phonon DOS of graphene becomes smaller, representing the stronger restriction on atoms' vibration due to covalent bonds. As a result, the phonon DOS of the adjacent Si atoms layer obviously has a better match with that of graphene than that of the adjacent C atoms layer at the frequency range below 25 THz. However, the situation is reversed at higher frequencies.

The overlap area of phonon DOS on both sides is further analyzed for better understanding of our calculation results. A variable which is defined as $\delta = \int A(f)fdf$ is computed and listed in Table 3, where $A(f)$ is the intersected area at the frequency of f. The meaning of the parameter A(f) is the intersected area at the frequency of f, which can be expressed mathematically $A(f) = \int |DOS_G(f) - DOS_{SiC}(f)|df$ where DOS means the phonon DOS. The area integration is proportional to the amount of energy transported across the interface by phonons at these frequency intervals. The computed values for graphene on C-terminated SiC are 41743 and 49898, respectively, in the case of van der Waals interaction and covalent interaction while for graphene on Si-terminated SiC are 38541 and 45390, respectively. The larger δ value calculated at the C-terminated interface than that of Si-terminated interface under both van der Waals and covalent bonding interfaces partially explains the larger ITC between graphene and C-terminated SiC, although the C–Si energy constant of LJ potential is nearly a factor of 3 larger than the C–C energy constant. It needs to be noted that one cannot compare δ between van der Waals and covalent bonding interfaces because other factors determining phonon transmission probability such as the phonon modes, wave factors, and the effects of different anharmonic interactions are not the same for different atomic interactions. The scattering of phonon to the interface is more likely inelastic for the

Table 3 Comparison of the transmitted phonon energy through the interface: the integration of the overlap area multiplied by the corresponding frequency in phonon DOS of the interface materials

$\delta = \int A(f)fdf$	Covalent bonded	Van der Waals interaction
C-terminated	49898	41743
Si-terminated	45390	38541

covalent system and elastic for the van der Waals system. Thus, the direct comparison of the overlap area between two interaction forces is not applicable. The introduction of overlap area of phonon DOS can be used to separately study the different atom-terminated faces (C and Si) for the same interaction force and thus figure out the mechanism why the C-terminated SiC substrate would give larger thermal conductance. From the above analysis, we can attribute the variance of ITC between graphene and SiC to the strength of the interfacial interaction, the structural influence on the number of covalent bonds, and from the spectral viewpoint the difference of phonon DOS of graphene and SiC.

3.2 Effect of the crystallinity of substrate

Phonon transmission through graphene interfaces is affected not only by the atomic interactions but also by the structure of substrate. Our study is extended by comparing the thermal transport across graphene/crystalline SiC (c-SiC) and graphene/amorphous SiC (a-SiC) interfaces. Figure 6 (a) shows the schematic of the structure of a-SiC and c-SiC, and corresponding RDF curves. The amorphous structure can be evidenced by no periodic peaks in the RDF of a-SiC (black line). Similar MD configuration as crystalline structures, ITC can be calculated through the temperature difference across the interface combined with the heat flux applied on it. The structure of the graphene/a-SiC interface as well as the temperature rise after heat flux is applied is shown in Fig. 6(b). The ITC between graphene and a-SiC is computed as $3.49 \pm 0.08 \times 10^7$ W/(m^2·K), which is larger than both graphene/C-terminated c-SiC and graphene/Si-terminated c-SiC interfaces.

Since the surface of the a-SiC adjunct to graphene is a mixture of Si atoms and C atoms, the value of ITC is expected to be between that of graphene/C-terminated c-SiC and that of graphene/Si-terminated c-SiC. However, from our simulation, this speculation is not the case. In fact, the higher ITC at a disordered interface was observed before by English et al. [42], in whose work the effect of different levels of disorder on the interfacial thermal conductance was investigated and the medium level of disorder was proven to be most beneficial to the interfacial thermal transport. In our model, the graphene is a single-layer film and unchanged, while the substrate is changed to be amorphous. Thus, our results are innovative and only suitable for our model or for other graphene/substrate systems The abnormal phenomenon can be explained by the difference in vibrational properties of crystalline solid and amorphous solid. Phonon DOS is plotted for understanding this phenomenon. As shown in Fig. 7, the phonon DOS of a-SiC is much smoother than the phonon DOS of either adjacent C atoms or Si atoms under van der Waals interaction. The phonon energy does not concentrate at a narrow frequency range from 10 to 20 THz and from 30 to 40 Hz like those of c-SiC (red and blue lines), but span the whole interval of 0–60 THz. The wide phonon DOS allows larger possibility for phonon transmission across the interface and improves the overlap area of the phonon DOS of graphene and that of a-SiC. The result shows that the overlap is 23.5 % higher than that of graphene/C-terminated c-SiC interface and 33.7 % higher than that of graphene/Si-terminated c-SiC system, which explains our

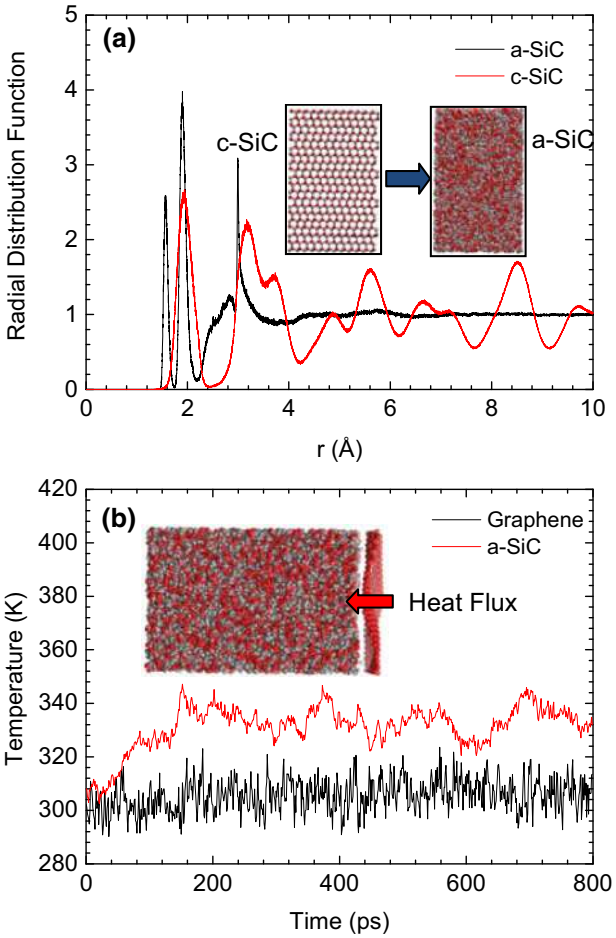

Fig. 6 **a** Radial distribution functions and the structure of crystalline SiC (c-SiC) and amorphous SiC (a-SiC); **b** the schematic of the calculation of ITC between a-SiC and graphene, in which the lines stand for the temperature evolution with time

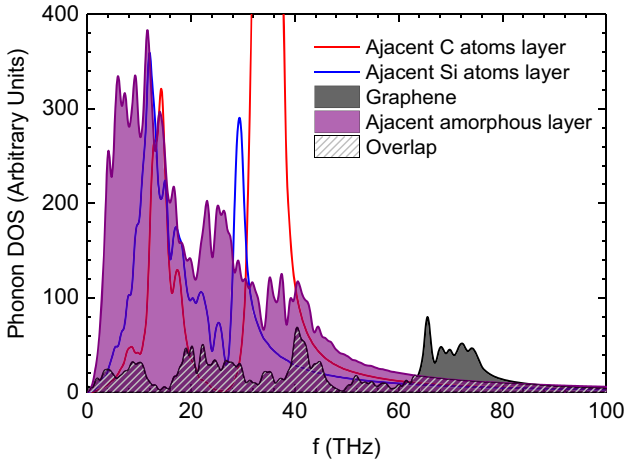

Fig. 7 Phonon DOS of graphene, adjacent atoms layer on C-terminate SiC, on Si-terminate SiC, and on a-SiC under the van der Waals interfacial interaction

simulated result that the ITC across amorphous interface is larger than crystalline interfaces. Besides, the rough surface feature of amorphous solids may be partly responsible for the improved ITC, which has been verified by Zhang et al. that the subnanoscale roughness might be good for interfacial energy coupling [43].

The fact that the ITC of graphene/a-SiC is larger than that of graphene/c-SiC gives us a new interpretation of the thermal transport in amorphous structure. In traditional understanding, amorphous solids transport heat far slower than its crystalline forms due to the short phonon mean free path. However, when it comes to the interfacial thermal transport where the intrinsic phonon mean free path of one component at the interface does not dominate the thermal conductance, the situation becomes different. Because of the wide phonon channels opened by the smooth phonon DOS of a-SiC, the heat dissipates from graphene to a-SiC could be faster than to c-SiC. This result indicates that the interface thermal transport can be further modified by changing crystalline structures of substrate.

4 Conclusion

In summary, the interfacial thermal transport between graphene and 4H-SiC is studied considering the effects of interatomic interaction, the terminated face of SiC, and the crystallinity of substrate. The interatomic interaction between graphene and SiC has significant effect on the ITC, and two magnitudes of improvement for covalent-bonded graphene interface than that of van der Waals interaction are obtained. The ITC of graphene/C-terminated SiC is larger than graphene/Si-terminated SiC, which is attributed to the stronger bond strength of C–C than that of C–Si. The results emphasize the importance of direct synthesis of graphene-based transistor from epitaxial graphene to meet the strict demand for high-density heat dissipation. The larger ITC of graphene/a-SiC than graphene/c-SiC shows that amorphous solids might be better for interfacial thermal transport of atomic structures.

Acknowledgments This work is supported by National Natural Science Foundation of China (No. 51206124, No. 51428603) and SRF for ROCS, SEM.

References

1. A.K. Geim, Science **324**(5934), 1530 (2009)
2. A.K. Geim, K.S. Novoselov, Nat. Mater. **6**(3), 183 (2007)
3. A.A. Balandin, S. Ghosh, W. Bao, I. Calizo, D. Teweldebrhan, F. Miao, C.N. Lau, Nano Lett. **8**(3), 902 (2008)
4. J. Hu, X. Ruan, Y.P. Chen, Nano Lett. **9**(7), 2730 (2009)
5. J. Zhang, X. Huang, Y. Yue, J. Wang, X. Wang, Phys. Rev. B **84**(23), 235416 (2011)
6. K.M.F. Shahil, A.A. Balandin, Nano Lett. **12**(2), 861 (2012)
7. M. Freitag, M. Steiner, Y. Martin, V. Perebeinos, Z. Chen, J.C. Tsang, P. Avouris, Nano Lett. **9**(5), 1883 (2009)
8. J.H. Seol, I. Jo, A.L. Moore, L. Lindsay, Z.H. Aitken, M.T. Pettes, X. Li, Z. Yao, R. Huang, D. Broido, N. Mingo, R.S. Ruoff, L. Shi, Science **328**(5975), 213 (2010)
9. M.M. Sadeghi, I. Jo, L. Shi, Proc. Nat. Acad. Sci. **110**(41), 16321 (2013)
10. J. Chen, G. Zhang, B. Li, Nanoscale **5**(2), 532 (2013)
11. Z.-Y. Ong, E. Pop, Phys. Rev. B **84**(7), 075471 (2011)
12. B. Qiu, X. Ruan, Appl. Phys. Lett. **100**(19), 193101 (2012)
13. Z. Chen, W. Jang, W. Bao, C.N. Lau, C. Dames, Appl. Phys. Lett. **95**(16), 161910 (2009)
14. K.F. Mak, C.H. Lui, T.F. Heinz, Appl. Phys. Lett. **97**(22), 221904 (2010)
15. Y.K. Koh, M.-H. Bae, D.G. Cahill, E. Pop, Nano Lett. **10**(11), 4363 (2010)
16. X. Tang, S. Xu, J. Zhang, X. Wang, ACS Appl. Mater. **6**(4), 2809 (2014)
17. X. Yu, L. Zhang, X. Song, T. Xi, Y. Zhao, J. Liu, X. Yang, M. Chen, P. Yang, Int. J. Mater. Struct. Intergr. **6**(1), 65 (2012)
18. P.E. Hopkins, M. Baraket, E.V. Barnat, T.E. Beechem, S.P. Kearney, J.C. Duda, J.T. Robinson, S.G. Walton, Nano Lett. **12**(2), 590 (2012)
19. C. Shu-Wei, K.N. Arun, J.B. Markus, J. Phys-Condens, Matter. **24**(24), 245301 (2012)
20. L. Chen, Z. Huang, S. Kumar, Appl. Phys. Lett. **103**(12), 123110 (2013)
21. K.V. Emtsev, A. Bostwick, K. Horn, J. Jobst, G.L. Kellogg, L. Ley, J.L. McChesney, T. Ohta, S.A. Reshanov, J. Röhrl, Nat. Mater. **8**(3), 203 (2009)
22. M. Sprinkle, M. Ruan, Y. Hu, J. Hankinson, M. Rubio-Roy, B. Zhang, X. Wu, C. Berger, W. De Heer, Nat. Nanotechnol. **5**(10), 727 (2010)
23. R. Mao, B.D. Kong, K.W. Kim, T. Jayasekera, A. Calzolari, M. Buongiorno, Nardelli. Appl. Phys. Lett. **101**(11), 113111 (2012)
24. H. Wang, J. Gong, Y. Pei, Z. Xu, ACS Appl. Mater. **5**(7), 2599 (2013)
25. A. Mattausch, O. Pankratov, Phys. Rev. Lett. **99**(7), 076802 (2007)
26. R. Wilson, D.G. Cahill, Phys. Rev. Lett. **108**(25), 255901 (2012)

27. S. Hertel, D. Waldmann, J. Jobst, A. Albert, M. Albrecht, S. Reshanov, A. Schöner, M. Krieger, H.B. Weber, Nat Commun **3**, 957 (2012)
28. Z. Xu, M.J. Buehler, J Phys-Condens Mat. **24**(47), 475305 (2012)
29. V. Sorkin, Y.W. Zhang, Phys. Rev. B **82**(8), 085434 (2010)
30. M. Li, Y. Yue, RSC Adv. **4**(44), 23010 (2014)
31. J. Tersoff, Phys. Rev. B **39**(8), 5566 (1989)
32. J. Tersoff, Phys. Rev. B **49**(23), 16349 (1994)
33. C. Tang, L. Meng, H. Xiao, J. Zhong, J. Appl. Phys. **103**(6), 063505 (2008)
34. L. Lindsay, D.A. Broido, Phys. Rev. B **81**(20), 205441 (2010)
35. S. Plimpton, J. Comput. Phys. **117**(1), 1 (1995)
36. S. Nosé, J. Chem. Phys. **81**(1), 511 (1984)
37. A.M.V.D. Zande, R.A. Barton, J.S. Alden, C.S. Ruiz-Vargas, W.S. Whitney, P.H.Q. Pham, J. Park, J.M. Parpia, H.G. Craighead, P.L. McEuen, Nano Lett. **10**(12), 4869 (2010)
38. J.E. Huheey, E.A. Keiter, R.L. Keiter, O.K. Medhi, Inorganic chemistry: principles of structure and reactivity. (Pearson Education India, 2006), pp. A-21
39. T. Luo, J.R. Lloyd, Adv. Funct. Mater. **22**(12), 2495 (2012)
40. E.T. Swartz, R.O. Pohl, Rev. Mod. Phys. **61**(3), 605 (1989)
41. B. Li, J. Lan, L. Wang, Phys. Rev. Lett. **95**(10), 104302 (2005)
42. T.S. English, J.C. Duda, J.L. Smoyer, D.A. Jordan, P.M. Norris, L.V. Zhigilei, Phys. Rev. B **85**(03), 035438 (2012)
43. J. Zhang, Y. Wang, X. Wang, Nanoscale **5**(23), 11598 (2013)
44. C.-C. Chen, Z. Li, L. Shi, S.B. Cronin, Appl. Phys. Lett. **104**(8), 081908 (2014)
45. Y. Yue, J. Zhang, X. Wang, Small **7**(23), 3324 (2011)